Spontaneous Emission Study of the Femtosecond Isomerization Dynamics of Rhodopsin

Gerd. G. Kochendoerfer and Richard A. Mathies*

Department of Chemistry, University of California, Berkeley, California 94720

Received: February 21, 1996; In Final Form: June 14, 1996[⊗]

The spontaneous emission spectra and yields of the visual pigment rhodopsin and its 9-*cis* retinal analog isorhodopsin have been measured following excitation at 472.7, 514.5, and 568.2 nm. The fluorescence quantum yields are $(0.9 \pm 0.3) \times 10^{-5}$ for rhodopsin and $(1.8 \pm 0.7) \times 10^{-5}$ for isorhodopsin. By use of a Strickler−Berg analysis, these quantum yields correspond to excited electronic state lifetimes of 50 and 100 fs for rhodopsin and isorhodopsin, respectively. The fluorescence spectra also undergo a blue-shift of ∼1800 cm^{-1} upon shifting the excitation wavelength from 568.2 to 472.7 nm. This is consistent with the idea that the emission arises from unrelaxed, nonstationary vibrational states. For rhodopsins, there is a correlation among these rapid initial nuclear dynamics out of the Franck−Condon region, the rapid photoisomerization rates, and the high isomerization quantum yields. These results support a new mechanism for the isomerization reaction dynamics in visual pigments where the reaction efficiency is mechanistically linked to the reaction rate through a dynamic Landau−Zener tunneling process.

Introduction

In the primary event in vision, the 11-*cis* retinal chromophore of the photoreceptor protein rhodopsin undergoes a *cis*-to-*trans* isomerization about its C_{11}═C_{12} double bond to form the primary photoproduct photorhodopsin, which relaxes to bathorhodopsin.[1−3] Isorhodopsin, a visual pigment analog containing a 9-*cis* retinal chromophore, isomerizes around its C_9═C_{10} double bond, producing a photoproduct that is very similar to the photoproduct of rhodopsin.[1,4] The isomerization quantum yield for isorhodopsin is 0.22, a factor of 3 lower than that of rhodopsin (0.67).[5,6] Early time-resolved absorption and fluorescence measurements were not able to resolve the fundamental processes but put upper limits of several picoseconds on the photoproduct appearance time[7] and 12 ps on the fluorescence lifetime.[8,9] The fluorescence quantum yields of bovine, squid, and isorhodopsin have also been used to place limits on the fluorescence lifetimes through a Strickler−Berg analysis.[9] The fluorescence quantum yield of these rhodopsins (∼10^{-5}) in combination with the radiative lifetimes suggested that the excited state lifetime was subpicosecond, indicative of an ultrafast reaction. Additional evidence for an ultrafast reaction came from a resonance Raman intensity analysis by Loppnow and co-workers, who observed several highly displaced low-frequency torsional modes.[10] From the absolute cross-section analysis they calculated a 35 fs departure of the excited state wave packet from the Franck−Condon region and predicted that the isomerization could occur as fast as 200 fs.

The advent of femtosecond absorption spectroscopy provided the opportunity to directly time-resolve the dynamics of the primary event in vision. Schoenlein et al. showed that the initial isomerization process is complete in only 200 fs.[11] Although this result was challenged by Yan et al. who interpreted their data in terms of a 3 ps photoproduct appearance time,[12] a complete femtosecond time-resolved absorption study by Peteanu et al. with higher time-resolution and a wider probe-wavelength range corroborated the photoproduct appearance time of 200 fs.[13] The 9-*cis* to all-*trans* isomerization of isorhodopsin was subsequently shown to be complete in 600 fs.[14] These studies provided the first evidence that there is a correlation between rapid reaction rates and high reaction quantum yields.

Current models of rhodopsin's excited state dynamics can be differentiated from earlier work by the time-ordering of vibrational dephasing and relaxation relative to the reactive motion (for a review see ref 15). Traditionally, we expect vibrational dephasing and relaxation to precede reactive surface crossing (Kasha's rule). The recent observation of vibrational oscillations in the rhodopsin photoproduct absorption provides direct evidence that this reaction is vibrationally coherent and that condensed phase photochemistry can be as fast or faster than vibrational dephasing.[16] It is thus clear that an improved understanding of the *very early dynamics* of the rhodopsin isomerization process is crucial for understanding the high efficiency and rate of the isomerization. This prompted us to reinvestigate the fluorescence spectra and quantum yields of rhodopsin and isorhodopsin.

Classically, the total fluorescence emission is a measure of the efficiency with which nonradiative processes compete with the radiative return of a vibrationally relaxed excited state population to the ground-state surface. For ultrafast reactions, the fluorescence quantum yield and the dependence of the fluorescence spectra on excitation wavelength are most intuitively interpreted and modeled through consideration of the dynamic evolution of nonstationary vibrational states on the excited state surface as illustrated in Figure 1. In the wave packet representation of molecular spectroscopy,[17] photoexcitation projects a replica of the ground-state nuclear distribution (a wave packet) onto the excited state potential surface. Owing to the steepness of this surface, the wave packet moves rapidly out of the Franck−Condon region and gains considerable momentum on its way to the crossing region or transition state between the excited and ground state. The fluorescence emitted by the moving wave packet is shown by the bold vertical arrow. Since the reaction rate is faster than typical vibrational dephasing and relaxation times,[18] the emission is expected to occur from nonstationary, vibrationally unrelaxed excited state populations. This suggests that the spectra might depend on the excitation wavelength. The evolution along the reaction coordinate also causes a change in the electronic wave function and hence a decay of the transition dipole moment between the excited and ground state that is expected to lead to a loss of emission. In

* To whom correspondence should be addressed.

[⊗] Abstract published in *Advance ACS Abstracts,* August 1, 1996.

S0022-3654(96)00509-6 CCC: $12.00

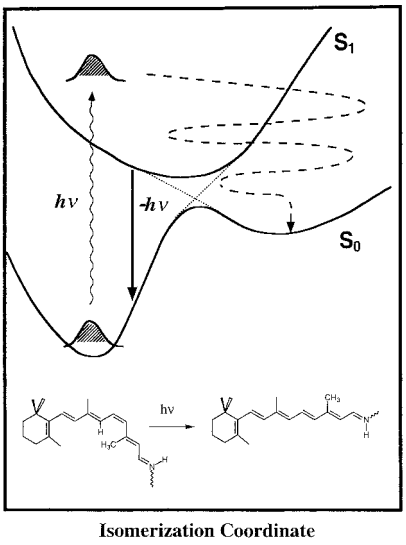

Figure 1. Schematic of the electronic potential energy surfaces of rhodopsin indicating the origin of the dynamic fluorescence emission and the vibrationally coherent mechanism for the primary event in vision. The excited state wave packet rapidly moves out of the Franck−Condon region toward the transition state. Fluorescence emission (bold vertical arrow) predominantly occurs during the early evolution of the wave packet while it is still strongly dipole-coupled to the ground state. Dotted lines indicate the diabatic surfaces along which the isomerization occurs. The molecule coherently tunnels to the photoproduct ground-state surface where it vibrationally relaxes and cools.

this circumstance, fluorescence spectroscopy specifically probes the initial dynamics of the excited state wave packet and monitors the departure of the excited state wave packet from the Franck−Condon region. The fluorescence spectra therefore represent an important constraint on simulations of the excited state potential surface and the dynamics of the rhodopsin isomerization.

In this paper, we have measured the full spontaneous emission spectra and fluorescence quantum yields of rhodopsin and isorhodopsin following excitation at three different excitation wavelengths. The fluorescence quantum yields are found to be very low ($\sim 10^{-5}$), and the spectra are significantly excitation wavelength dependent, consistent with the idea that the emission is from nonstationary vibrational states. These data support the idea that rhodopsin exhibits rapid torsional deformation in 50−100 fs to a region on the excited state potential surface that is no longer strongly dipole coupled to the ground-state surface. Comparison of these data with the isomerization quantum yields of rhodopsin and isorhodopsin demonstrates that there is a correlation between rapid *initial* dynamics, a high isomerization quantum yield, and a rapid *overall* reaction rate. This work provides further support for a new mechanism for the primary event in vision where nonstationary vibrational states mediate dynamic reaction potential surface crossing.

Materials and Methods

Sample Preparation. Rod outer segments (ROS) were isolated from 100 bovine retinas (J. A. Lawson, Lincoln, NE) by sucrose flotation followed by sucrose density gradient centrifugation as described previously.[19] To avoid contamination of the sample with fluorescent impurities, glassware was washed with dilute acid and rinsed with deionized water. The yield was typically 12−15 nmol of rhodopsin/retina ($\epsilon = 40\,600$ M^{-1} cm^{-1} at 500 nm). The ROS were lysed in water and solubilized in 15 mL of 5% Ammonyx-LO (Exciton, Dayton, OH). The resulting rhodopsin solution was then loaded on a hydroxylapatite column.[20] The protein was eluted with a phosphate step gradient (30 to 150 mM PO_4^{3-}, pH 7). Most of the rhodopsin was eluted in the first 25 mL of the high-phosphate elution buffer at concentrations of 20−55 μM. Only these fractions were used in the fluorescence experiments, since concentrating the more dilute fractions resulted in increased background fluorescence. Samples with increased background fluorescence did not alter the magnitude of the measured rhodopsin fluorescence because we always subtract a bleached fluorescence blank. However, it was desirable to reduce the background to improve the precision of the measurement. Final solutions were between 0.8 and 1.3 OD/cm (150 mM PO_4^{3-}, 1% Ammonyx-LO, <5 mM NH_2OH). Rhodopsin was converted to isorhodopsin by irradiation of samples frozen at 77 K with 568 nm light (70 mW/cm^2) from a Kr^+ laser (Spectra Physics 2020-11) for 30 min.[21] The almost complete conversion of rhodopsin to isorhodopsin was verified by the shift of the absorption maximum from 500 to 485 nm. Resonance Raman spectra of the isorhodopsin samples did not reveal any residual rhodopsin (<5%).

Fluorescence Spectroscopy. Fluorescence spectra of rhodopsin and isorhodopsin were obtained with 10−15 mL solutions having an absorbance of 0.8−1.3 OD/cm at 500 and 485 nm, respectively. The fluorescence was excited by focusing the laser beam with a 100 mm focal length spherical lens on the 0.6 mm diameter capillary containing the flowing pigment solution. Laser excitation was obtained with Kr^+ and Ar^+ ion lasers (Spectra-Physics, Mountain View, CA, Models 2020). The laser power (0.5−5 mW), flow rate (300−500 cm/s), and beam waist (32 μm) were chosen to minimize the effects of photolysis on the fluorescence spectra (photoalteration <0.1).[22] The extent of bulk photolysis was monitored by taking absorption spectra prior to each scan. No pigment fluorescence spectra were taken after more than 33% of the sample had been bleached.

The total emission of the sample was detected with a photon-counting detector coupled to a Spex 1401 double monochromator. Two different monochromator settings were used. To obtain broad, low-resolution fluorescence data with a high S/N ratio, the exit slit was opened to a 30 cm^{-1} detection band-pass (1500 μm), with the entrance slit at 300 μm, and a scan speed of 33 cm^{-1}/s. To obtain high-resolution Raman spectra, the detection band-pass was reduced to 4 cm^{-1} (300 μm) and the spectra scanned at 4 cm^{-1}/s. The decrease in photon flux upon narrowing the slits is calibrated by comparison of two bleach spectra taken with wide and narrow exit slits. The emission intensity decreased by a factor of 8 upon reduction of the exit slit width. Data collection was performed with a PDP 11/23 computer. Each spectrum has been divided by a tungsten halogen lamp spectrum (Eppley Lab. Inc., Newport, RI) to correct for the spectrometer response and detection sensitivity.

Methods for Determination of the Fluorescence Quantum Yield. The absolute fluorescence quantum yield of rhodopsin was determined by comparing the integrated fluorescence emission both to the integrated Raman intensity of the ethylenic stretch of rhodopsin and to the intensity of the integrated water Raman lines at $\sim$3300 cm^{-1}. The absolute Raman cross sections of both Raman lines have been determined previously.[10,23] The determination of the ratio of the fluorescence intensity I_f to the rhodopsin Raman intensity I_R and the knowledge of the absolute ethylenic Raman cross section σ_R allow for the calculation of the absolute fluorescence cross section σ_f. For polarized emission from the same molecule, σ_f and σ_R are related by

$$\sigma_f = \frac{I_f}{I_R}\sigma_R \qquad (1)$$

The fluorescence quantum yield Φ_f is defined as

$$\Phi_f = \sigma_f/\sigma_a \tag{2}$$

where σ_a is the absorption cross section. Therefore, the fluorescence quantum yield is given by

$$\Phi_f = \frac{I_f}{I_R}\frac{\sigma_R}{\sigma_a} \tag{3}$$

The absolute Raman cross section σ_R of the ethylenic line of rhodopsin at 514.5 nm is $(3180 \pm 500) \times 10^{-10}$ Å^2/molecule.[10] The extinction coefficient of rhodopsin at 515 nm is 38 000 M^{-1} cm^{-1}, yielding an absorption cross section of 1.45 Å^2/molecule.

An alternative method for determining the fluorescence quantum yield is to compare the total fluorescence emission to the water Raman bands. The differential Raman cross section of the water bands is 1.1×10^{-14} Å^2/sterad/molecule at 514.5 nm.[23] Corrections must be made for the difference in concentration and depolarization ratio between the water Raman scattering and the fluorescence emission. The expression is

$$\Phi_f = \frac{I_f}{I_R}\frac{\sigma_{water}}{\sigma_a}\frac{c_{water}}{c_{rho}}\Delta \tag{4}$$

where σ_{water} is the absolute Raman cross section[24] of the water bands at 514.5 nm (1.1×10^{-13} Å^2 /molecule) and c_{water} and c_{rho} are the concentrations of water and rhodopsin, respectively. In this expression Δ is a correction factor accounting for the different depolarization ratios ρ of the water Raman bands and the fluorescence emission, which is given by

$$\Delta = \left(\frac{1+2\rho}{1+\rho}\right)_{fluo}/\left(\frac{1+2\rho}{1+\rho}\right)_{water} \tag{5}$$

The ultrashort fluorescence lifetime of rhodopsin suggests that its depolarization ratio should be 0.33. This is close to our experimentally determined value of 0.35 ± 0.1 (data not shown). By use of the 0.33 value, the correction factor Δ is 1.1.

Results

Rhodopsin Emission Data. Figure 2A presents the low-resolution total emission spectrum of rhodopsin excited at 514.5 nm. A broad emission band extending from 12 000 to 19 000 cm^{-1} overlaps with the unresolved water Raman bands around 16 000 cm^{-1} and 3 bands assignable to groups of rhodopsin Raman lines, including the hydrogen out-of-plane lines around 18 500 cm^{-1}, the fingerprint lines around 18 300 cm^{-1}, and the ethylenic line around 17 800 cm^{-1}. Since accurate integration of the ethylenic Raman line is not possible from this low-resolution scan, the exit slit of the spectrograph was reduced and a high-resolution scan of the ethylenic region was taken (inset in Figure 2). Finally, to discriminate between background fluorescence due to nonbleachable impurities and scattering, and intrinsic fluorescence from the highly photosensitive pigment, the pigment component of the sample was *completely* bleached by turning on the roomlight for $\leq$5 min until *all* the 500 nm rhodopsin absorbance was eliminated. Then a low-resolution spectrum was taken under the same conditions as for the unbleached sample. The stability of the background emission over several scans suggests that the background emission is indeed due to residual impurities that are not significantly photosensitive. This spectrum, displayed in Figure 2B, does not contain contributions from the rhodopsin Raman lines but exhibits only a broad envelope of impurity emission and the unresolved water Raman bands. Figure 2C presents the difference between the unbleached and the bleached spectrum. The broad intensity-corrected fluorescence band has a maximum at 650 nm. The narrow features seen in the difference spectrum are the rhodopsin resonance Raman bands described above.

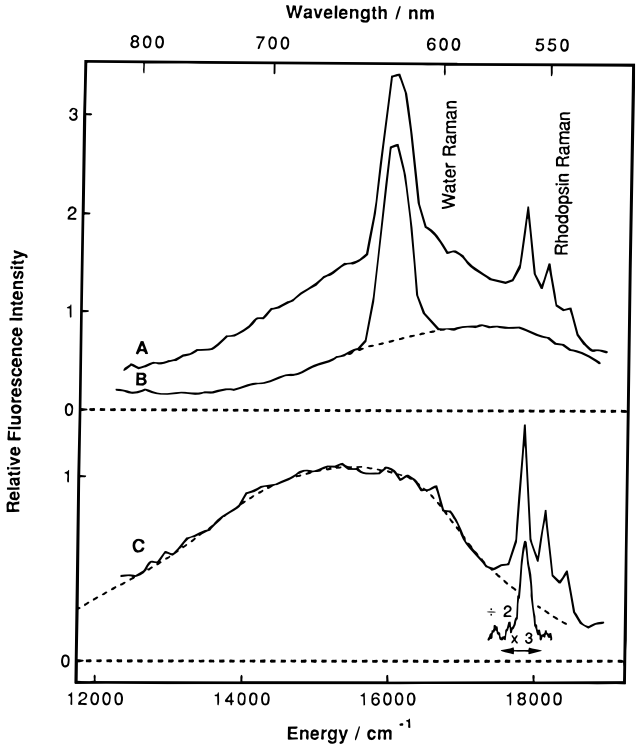

Figure 2. (A) Low-resolution intensity-corrected emission spectrum of rhodopsin excited with 0.6 mW of 514.5 nm light (initial absorbance = 1 OD/cm at 500 nm, step size = 100 cm^{-1}, entrance slit = 300 μm, and exit slit = 30 cm^{-1}). (B) Emission of the rhodopsin sample after bleaching with white light. (C) Difference between A and B. The inset presents a high-resolution scan of the ethylenic line of rhodopsin at 1549 cm^{-1} (step size = 4 cm^{-1}, entrance slit width = 300 μm, exit slit = 4 cm^{-1}). The emission intensity decreased by a factor of 8 upon reduction of the exit slit width from 30 to 4 cm^{-1}. The high-resolution scan in the inset has been multiplied by this factor to normalize it to the low-resolution difference spectrum. Note that the scale of C has been expanded by a factor of 2. All spectra are averages of two scans. The dashed lines in B is the background subtracted during integration of the water Raman band. The dashed line in C is the fit of the rhodopsin fluorescence spectrum used for the integration.

The determination of the absolute fluorescence quantum yield requires an accurate integration of the fluorescence spectrum. Therefore, the broad feature in the difference spectrum was fit with a sixth-order polynomial to estimate its area (see Figure 2C). To determine the integrated area of the water Raman bands, a polynomial background was first subtracted from the total bleach emission spectrum prior to integration (see Figure 2B). To determine the integrated area of the rhodopsin ethylenic Raman band, a bleached background was subtracted from the ethylenic Raman spectrum prior to integration. The intensity of the rhodopsin Raman line was then corrected for the decreased photon flux due to the closing of the slits as described above. The amount of partial bleaching at the time of each scan is determined by the decrease in absorbance relative to the unbleached sample. The intensities of the fluorescence emission and the Raman scattering from the partially bleached samples were then corrected to the value for an unbleached sample, yielding an absolute ratio of the fluorescence intensity relative to the Raman intensity. The experimental ratio of the fluorescence intensity I_f to the total Raman intensity I_R of the ethylenic line for rhodopsin is 50 ± 15. Equation 3 then yields

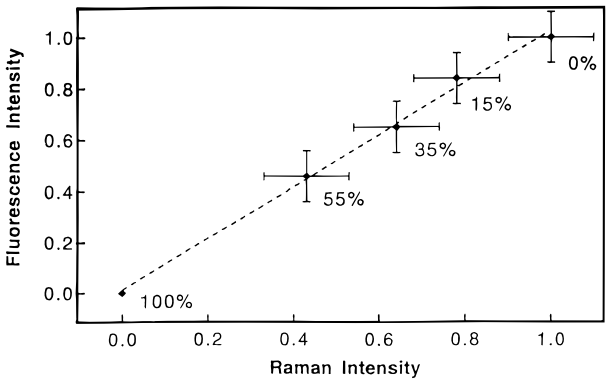

Figure 3. Plot of the integrated fluorescence intensity vs the integrated ethylenic Raman intensity of rhodopsin after different amounts of bleaching. Spectra were excited with 0.6 mW of 514.5 nm light. Experimental conditions and slit-settings are described in Figure 2. For each data point, a broad low-resolution and a high-resolution scan of the ethylenic line were taken consecutively. The amount of bleaching, determined by the decrease in absorbance relative to the unbleached sample, is indicated. The fitted linear regression line has a slope of 1.01 ($R = 0.998$).

an absolute fluorescence quantum yield of $(0.9 \pm 0.3) \times 10^{-5}$ for rhodopsin. The experimentally determined ratio of the integrated rhodopsin fluorescence I_f and the water Raman intensity I_R with excitation at 514.5 nm is 4.5 ± 1.2 for a solution having an optical density of 1. Equation 4 then yields a fluorescence quantum yield of $(0.7 \pm 0.3) \times 10^{-5}$ for rhodopsin, in satisfactory agreement with the value derived from the rhodopsin Raman intensities.

The extremely weak fluorescence of rhodopsin requires a careful analysis of the spectra to establish that we are not detecting emission from photochemical intermediates, stray light, or spurious background emission that is not due to rhodopsin. While the emission from rhodopsin is expected to depend linearly on the excitation power, the emission from intermediates is expected to increase quadratically with excitation power. Control experiments demonstrated that the observed emission increases linearly when the excitation power is raised by a factor of 2. This indicates that the emission does not stem from fluorescing intermediates. Figure 3 presents a plot of the integrated fluorescence intensity vs the integrated Raman intensity of the rhodopsin ethylenic stretch for the same sample after different amounts of bleaching. One expects a linear relationship between the two intensities. The data can be fit with a straight line intersecting the origin (slope = 1.01, $R = 0.998$). The absence of any deviation from linearity also suggests that no emission from a bleachable impurity is detected that is expected to decay at a different rate. Additionally, owing to rhodopsins' ultrashort fluorescence lifetime, one expects little change in the orientation of the emitting dipole after excitation and therefore strongly polarized emission. On the other hand, the background impurity emission is not necessarily polarized. We observe a depolarization ratio of 0.35 ± 0.1 over the whole wavelength range of the rhodopsin fluorescence. However, depending on the sample, the anisotropy of the background emission varied between 0.05 and 0.15 (data not shown). These results corroborate that the observed emission is intrinsic rhodopsin fluorescence.

Isorhodopsin Emission Data. Figure 4A presents the low-resolution total emission spectrum of isorhodopsin excited at 514.5 nm. A broad emission extending from 12 000 to 19 000 cm^{-1} is overlapped by the unresolved water Raman bands around 16 000 cm^{-1} and 3 bands assignable to groups of isorhodopsin Raman lines, including the hydrogen out-of-plane lines around 18 500 cm^{-1}, the fingerprint lines around 18 300 cm^{-1}, and the ethylenic line around 17 800 cm^{-1}. Figure 4B presents the low-resolution spectrum taken under the same conditions after bleaching with white light. It consists of a broad envelope of impurity emission and the unresolved water Raman lines. Figure 4C presents the difference between the unbleached and the bleached spectrum. The broad intensity-corrected fluorescence band has its maximum at 650 nm. The fluorescence spectra of isorhodopsin were also found to be linear in excitation power. Both polarization experiments and a plot of the integrated fluorescence intensity vs the integrated Raman intensity after different amounts of bleaching support the assignment of the difference spectrum to intrinsic isorhodopsin fluorescence (data not shown). The isorhodopsin emission and the water Raman bands were integrated and corrected following the same procedures described above for the rhodopsin spectra.

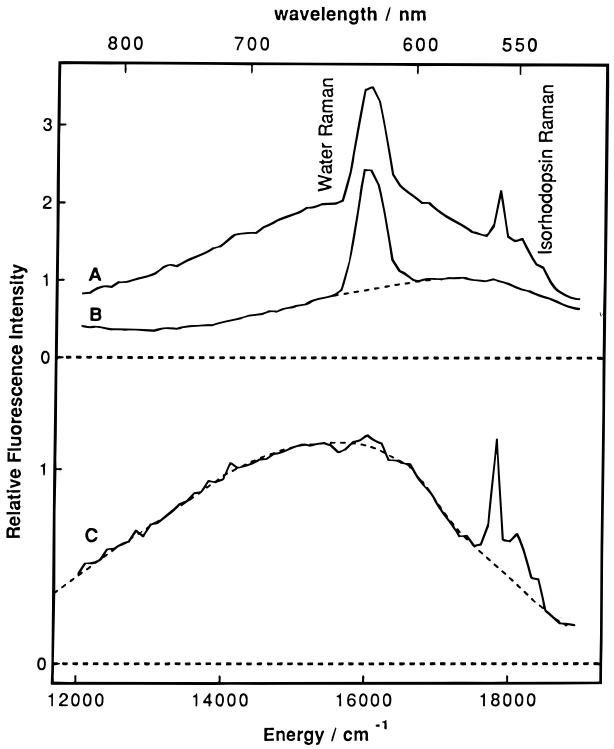

Figure 4. (A) Low-resolution emission spectrum of isorhodopsin excited with 0.6 mW of 514.5 nm light (initial absorbance = 1.1 OD/cm at 485 nm, step size = 100 cm^{-1}, entrance slit = 300 μm, and exit slit = 30 cm^{-1}). (B) Emission of the isorhodopsin sample after bleaching with white light. (C) Difference between A and B. Note that the scale of C has been expanded by a factor of 2. All spectra are averages of two scans. The dashed lines in B is the background subtracted during integration of the water Raman band. The dashed line in C is the fit of the isorhodopsin fluorescence spectrum used for the integration.

The fluorescence quantum yield of isorhodopsin was determined by comparison with the water Raman intensity, since the absolute Raman cross section of the ethylenic line of isorhodopsin is not available. The experimentally determined ratio of the rhodopsin fluorescence I_f and the water Raman intensity I_R with excitation at 514.5 nm is 11.2 ± 3.0 for a solution of an optical density of 1. Using eq 4, we calculate a fluorescence quantum yield of $(1.8 \pm 0.7) \times 10^{-5}$.

The determination of the ratio of the fluorescence quantum yield of isorhodopsin to that of rhodopsin is crucial for the comparison of their excited state dynamics. Although there is a large error in the determination of the *absolute* fluorescence yields, the determination of the *relative* fluorescence yields can be achieved with higher precision. These have been calculated from the respective ratios of the fluorescence spectrum of each protein to the corresponding water Raman lines. The corre-

TABLE 1: Radiative Lifetime, Fluorescence Lifetime, Isomerization Time, and Reaction Quantum Yield of Rhodopsin and Isorhodopsin[a]

	radiative lifetime (ns)	fluorescence lifetime (fs)	isomerization time (fs)	reaction quantum yield
rhodopsin	5 ± 2	50 ± 20	200[b]	0.67[c]
isorhodopsin	5 ± 2	100 ± 40	600[d]	0.22[e]

[a] The radiative lifetime τ_r was calculated from the Strickler−Berg formula $1/\tau_r = (2.888 \times 10^{-9}) n^2 \langle \nu_f^{-3} \rangle_{Av}^{-1} \int \epsilon(\nu)\, d\ln \nu$, with $\langle \nu_f^{-3} \rangle_{Av} = \int I(\omega)\, d\omega / \int I(\omega)/\omega^3\, d\omega$.[25] $I(\omega)$ is the fluorescence intensity at frequency ω. $\epsilon(\nu)$ is the extinction coefficient at the frequency ν. For the refractive index n we chose the value of water (1.33). $\langle \nu_f^{-3} \rangle_{Av}$ was calculated from the intensity-corrected fluorescence spectra of rhodopsin and isorhodopsin. The integral $\int \epsilon\, d\ln \nu$ was performed over the absorption spectrum of rhodopsin and isorhodopsin, respectively. [b] Schoenlein, R. W.; Peteanu, L. A.; Mathies, R. A.; Shank, C. V. *Science* **1991**, *254*, 412. [c] Wald, G. *Science* **1968**, *162*, 230. [d] Schoenlein, R. W.; Peteanu, L. A.; Wang, Q.; Mathies, R. A.; Shank, C. V. *J. Phys. Chem.* **1993**, *97*, 12087. [e] Hurley, J. B.; Ebrey, T. J.; Honig, B.; Ottolenghi, M. *Nature (London)* **1977**, *270*, 540.

sponding ratios are 4.5 ± 1.2 for rhodopsin and 11.2 ± 3.0 for isorhodopsin (averages and standard deviations of 5 experiments each). Error propagation yields a ratio of the fluorescence of isorhodopsin relative to rhodopsin of 2.5 ± 0.9.

Strickler−Berg Analysis. Classically, the emission quantum yield for an electronically excited state can be expressed as

$$\Phi_f = \left(\frac{k_r}{k_r + k_{nr}} \right) \tag{6}$$

where k_r^{-1} is the natural radiative lifetime τ_r and $(k_r + k_{nr})^{-1}$ is the lifetime τ of the excited state in the presence of nonradiative processes. The lifetime τ of the excited state can therefore be expressed as

$$\tau = \Phi_f \tau_r \tag{7}$$

By use of the Strickler−Berg relationship,[25] τ_r was calculated from the integrated absorption strength and the emission spectra at 568.2 nm. The resulting radiative lifetime was ~5 ns for both rhodopsin and isorhodopsin. By use of eq 7, this yields a lifetime of ~50 fs for rhodopsin and ~100 fs for isorhodopsin. The lifetimes, isomerization times, and quantum yields for rhodopsin and isorhodopsin are summarized in Table 1.

Excitation Wavelength Dependence. Figure 5 presents the emission spectra of rhodopsin and isorhodopsin obtained with excitation at 472.7, 514.5, and 568.2 nm. There is some uncertainty about the spectral shape at the blue edge of the spectra excited at 472.7 nm, since the background emission is increasing in the bleached relative to the unbleached sample. It is not clear whether this emission arises from oxidized membrane particles, retinal oxime, or impurities. Nevertheless, one clearly observes a blue-shift of the rhodopsin and isorhodopsin emission of ~1800 cm^{-1} upon shifting the excitation wavelength from 568.2 to 472.7 nm for both rhodopsin and isorhodopsin. The spectra at all excitation wavelengths are strongly Stokes-shifted. For both rhodopsin and isorhodopsin the shape of the emission spectrum with 568.2 nm excitation is close to a mirror image of the absorption spectrum. However, one observes a broadening of the emission spectra by ~750 cm^{-1} upon blue-shifting of the excitation wavelength. The spectra at all excitation wavelengths were integrated and corrected as described above. The absolute cross sections of the water Raman band at 472.7 and 568.2 nm were calculated from the values given by Champion,[23] invoking the ν^4-dependence of the off-resonance Raman scattering intensity.[26] The fluorescence quantum yields of rhodopsin and isorhodopsin were found to be independent of the excitation wavelength within the experimental error.

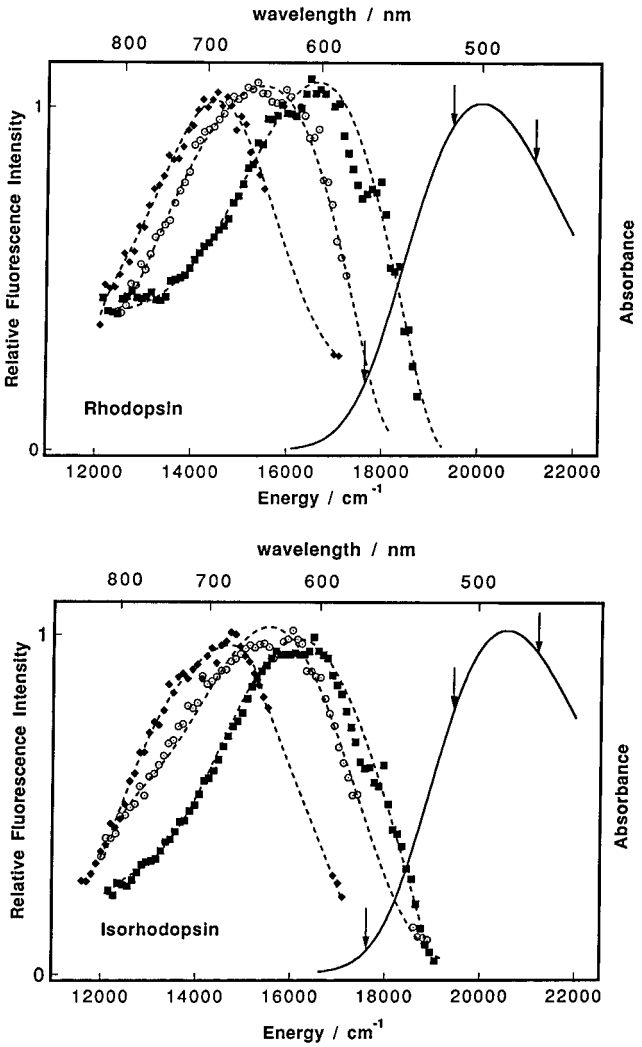

Figure 5. Absorption spectrum and emission spectra of rhodopsin (top panel) and isorhodopsin (bottom panel) after excitation at 472.7 nm (squares), 514.5 nm (circles), and 568.2 nm (diamonds). The experimental conditions are identical to those described in Figure 2, except that the laser power was 5 mW for the spectra excited at 568.2 nm. All spectra are averages of three to five experiments. For better display, the unresolved pigment Raman bands have been removed and the spectra are fit to a polynomial (dashed lines) and normalized to equal intensity. The arrows on the absorption spectrum indicate the respective excitation wavelengths.

Discussion

This is the first detailed study of the fluorescence yields and spectra of rhodopsins. Our spectra are red-shifted relative to the first study of rhodopsin fluorescence by Guzzo and co-workers, which suggested a λ_{max} of 575 nm.[27] However, Guzzo et al. also reported a fluorescence quantum yield (0.005) almost 3 orders of magnitude larger than the value found here. It therefore appears likely that Guzzo et al. observed emission from either impurities or photointermediates of rhodopsin. Our fluorescence quantum yield for rhodopsin is in satisfactory agreement with the studies by Doukas and co-workers who also reported that the fluorescence quantum yield of isorhodopsin is similar to that of rhodopsin.[8,9] However, our experiments clearly demonstrate that the fluorescence quantum yield for isorhodopsin is more than double that of rhodopsin. One explanation for this discrepancy might be the higher sensitivity and resolution of our detection method.

Our calculated fluorescence lifetimes are consistent with the results of femtosecond transient absorption experiments.[11,14] The 33 fs spectra of both rhodopsin and isorhodopsin exhibit a strong excited state absorption feature that rapidly decays to reveal the ground-state bleach. Although this feature has almost completely vanished after 100 fs for rhodopsin, it is still noticeable for isorhodopsin after 150 fs. Furthermore, isorhodopsin exhibits a strong stimulated emission band in the 33 and 150 fs delay spectra, while no such feature is discernible in the rhodopsin data. In transient absorption experiments the assignment of stimulated emission can sometimes be ambiguous owing to the overlap of the emission band with hot photoproduct and recovered ground-state absorption. However, spontaneous emission spectroscopy allows the unambiguous assignment of the emission spectrum to excited state population. The spontaneous emission spectrum of isorhodopsin obtained here confirms the assignment of the stimulated emission in the femtosecond transient absorption experiment of isorhodopsin.[14] Both the spontaneous emission data and the femtosecond stimulated emission data indicate that the lifetime of the excited state in the Franck−Condon region is significantly shorter in the case of rhodopsin than for isorhodopsin.

Interpretation of the Strickler−Berg Analysis. It is important to discuss the validity of the approach used to determine the apparent lifetimes of rhodopsin and isorhodopsin and how they should be interpreted. In the Strickler−Berg relationship between the absorption intensity and the fluorescence lifetime one assumes (1) that there is a strongly allowed absorption band, (2) that there is little coordinate dependence of the transition dipole moment (or little displacement in the excited state), and (3) that the emission comes from the lowest vibrational level of the lowest excited electronic state. Assumption 1 is certainly fulfilled in the case of rhodopsin. However, rhodopsin moves very rapidly out of the Franck−Condon region, which causes a change of the electronic character of the excited state with a concomitant change of the transition dipole moment.[28] This violates condition 2. The strong shift and broadening of the fluorescence as a function of excitation wavelength also indicate the presence of unrelaxed fluorescence, contrary to assumption 3.

Nevertheless, the literature contains examples of the usefulness of the Strickler−Berg relationship to determine fluorescence lifetimes even in the limit of very short excited state lifetimes. Shreve et al. investigated the excited state lifetime of β-carotene with femtosecond transient absorption spectroscopy and emission yield studies.[29] The value of ~200 fs for the excited state lifetime obtained from the decay of the excited state absorption of β-carotene nicely corresponds to the value found from the fluorescence quantum yield through the Strickler−Berg relationship. Recently, Kandori et al.[30] confirmed this fluorescence lifetime in femtosecond time-resolved fluorescence upconversion experiments.

In the case of photochemically active molecules, we interpret the Strickler−Berg excited state lifetime as a T_1 lifetime of the initially excited electronic state in the Franck−Condon region. We further assume that there is a coordinate-dependent transition dipole moment $\mu(Q)$ between the ground and first excited state[28] that rapidly changes as the molecule moves along the reaction coordinate and thereby acts to quench the spontaneous emission. An example of the successful application of the Strickler−Berg relationship to a reactive molecule with a barrierless excited state potential surface is bacteriorhodopsin. The Raman intensity analysis of bacteriorhodopsin showed that its all-*trans* retinal chromophore leaves the Franck−Condon region of the excited state within 30 fs.[31] The spontaneous emission quantum yield of bacteriorhodopsin ($(1 \pm 0.5) \times 10^{-4}$)[32,33] corresponds to a Strickler−Berg lifetime of ~700 fs.[33] This is consistent with the 500 fs excited state lifetime of bacteriorhodopsin determined by time-resolved stimulated emission and fluorescence upconversion experiments.[33,34] The applicability of this method to a protein chromophore undergoing large excited state geometry changes on a barrierless potential surface is the strongest evidence that our analysis yields a good qualitative determination of the time scale of the initial torsional dynamics.

Initial Torsional Dynamics. Recent studies have demonstrated a correlation between the reaction rate and the photochemical quantum efficiency of retinal proteins.[11,13,15] The experiment presented here allows us to investigate the correlation between efficient photochemistry and rapid initial excited stated dynamics. The fluorescence lifetime of rhodopsin (50 fs) is half that of isorhodopsin (100 fs). Measurements of the relative fluorescence yields of rhodopsin and isorhodopsin provide a more accurate value for the ratio of these fluorescence lifetimes of 2.5. In addition, the isomerization rate of rhodopsin (200 fs) is 3 times as fast as that of isorhodopsin (600 fs). These numbers correlate well with the 3-fold increased quantum yield for rhodopsin. This supports the idea that the rapid reaction rate of rhodopsin is determined by the geometric distortions that drive the molecule out of the Franck−Condon region of the excited state. The Raman spectrum of rhodopsin exhibits several highly displaced low-frequency modes at 93, 131, 260, and 568 cm^{-1}.[10,35] Rapid evolution along these low-frequency modes moves the 11-*cis* retinal chromophore out of the Franck−Condon region. Several effects then synergistically reduce the fluorescence quantum yield. First, the electronic character of the ground and excited state rapidly changes along the reaction coordinate through mixing of states of different symmetry.[36,37] This change causes a decrease in the transition dipole moment, reducing the emission intensity. In addition, the Einstein coefficient for spontaneous emission depends on the inverse cube of the energy gap ΔE. This gap between the states narrows rapidly along the reaction coordinate (see Figure 1), lowering the rate of fluorescence emission. Eventually, the rapid and efficient population transfer from the excited state to the photoproduct ground state depopulates the excited state and terminally quenches the fluorescence.

One possible driving force for the rapid initial dynamics in the 11-*cis* chromophore is the nonbonded interaction between the 10-H and 13-CH_3 group (see Figure 1). This steric interaction introduces a twist of the $C_{10}-C_{11}$ and $C_{12}-C_{13}$ single bonds as well as the isomerizing $C_{11}=C_{12}$ double bond in the ground state of the chromophore.[38] When the molecule is raised to the excited state surface, this nonbonded interaction will accelerate the molecule along the reaction trajectory once the torsional barrier has been reduced by optical excitation. This nonbonded interaction is not present in isorhodopsin, accounting for the slower initial dynamics. In support of this model, very recent experiments have shown that 13-desmethyl rhodopsin, a rhodopsin analog devoid of the 13-CH_3 group, isomerizes more slowly than rhodopsin and has a lower reaction quantum yield.[39] This analysis demonstrates that the rapid reaction rate and isomerization efficiency depend on the rapid initial torsional motion of the 11-*cis* retinal chromophore.

Vibrational Relaxation. The ordering of the time scales of vibrational dephasing and vibrational relaxation and cooling can have a fundamental impact on the mechanism of photochemical reactions. The significant shift and shape-change of the fluorescence spectra as a function of excitation wavelength demonstrate that the rhodopsin and isorhodopsin chromophores move out of the fluorescing region prior to complete vibrational

relaxation and/or cooling. This is consistent with the fact that the fluorescence lifetimes of rhodopsin and isorhodopsin are orders of magnitude shorter than typical vibrational dephasing and relaxation times.[18] The observation of vibrational coherence in the rhodopsin *photoproduct* several picoseconds after excitation also suggests that the emission observed here comes from molecules in vibrationally excited, nonstationary vibrational states.[16] These observations indicate that a successful model for the primary isomerization dynamics must consider the role of nonstationary excited vibrational states. In such a model, the excess photon energy is deposited in highly displaced vibrational modes. It appears likely that this excess vibrational energy along the reaction coordinate is carried in the Franck−Condon excited modes and that these modes are still preferentially excited for a significant distance along the reaction coordinate and probably even in the photoproduct ground state. This is consistent with the recent theoretical analysis of the absolute Raman intensities of rhodopsin[10,40] and modeling of picosecond time-resolved anti-Stokes Raman spectra of bacteriorhodopsin,[40] which suggested that the vibrational energy will stay in the initially excited vibrational modes during the reaction.

Conclusion

The fluorescence experiments presented in this paper demonstrate a correlation between the rapid initial nuclear dynamics out of the Franck−Condon region, the rapid photoisomerization rates, and the high isomerization quantum yields . The ultrashort fluorescence lifetimes further support a new mechanism for visual photochemistry in which nonstationary vibrational states play a critical role in the primary event according to a Landau−Zener surface-crossing mechanism.[41,42] It will now be interesting to model the fluorescence spectra of rhodopsin to get a more detailed picture of the nature of the emitting states and the shape of the electronic ground and excited state potential surfaces.

Acknowledgment. We thank Steve W. Lin, Andrew P. Shreve, Qing Wang, and Dave Wexler for helpful discussions and May Chan and Damon M. Kwan for expert assistance in rhodopsin preparation. This work was supported by a grant from the NIH (EY 02051).

References and Notes

(1) Yoshizawa, T.; Wald, G. *Nature* **1963**, *197*, 1279.
(2) Kandori, H.; Shichida, Y.; Yoshizawa, T. *Biophys. J.* **1989**, *56*, 453.
(3) Popp, A.; Ujj, L.; Atkinson, G. H. *J. Phys. Chem.* **1995**, *99*, 10043.
(4) Hayward, G.; Carlsen, W.; Siegman, A.; Stryer, L. *Science* **1981**, *211*, 942.
(5) Hurley, J. B.; Ebrey, T. G.; Honig, B.; Ottolenghi, M. *Nature (London)* **1977**, *270*, 540.
(6) Wald, G. *Science* **1968**, *162*, 230.
(7) Busch, G. E.; Applebury, M. L.; Lamola, A. A.; Rentzepis, P. M. *Proc. Natl. Acad. Sci. U.S.A.* **1972**, *69*, 2802.
(8) Doukas, A. G.; Lu, P. Y.; Alfano, R. R. *Biophys. J.* **1981**, *35*, 547.
(9) Doukas, A. G.; Junnarkar, M. R.; Alfano, R. R.; Callender, R. H.; Kakitani, T.; Honig, B. *Proc. Natl. Acad. Sci. U.S.A.* **1984**, *81*, 4790.
(10) Loppnow, G. R.; Mathies, R. A. *Biophys. J.* **1988**, *54*, 35.
(11) Schoenlein, R. W.; Peteanu, L. A.; Mathies, R. A.; Shank, C. V. *Science* **1991**, *254*, 412.
(12) Yan, M.; Manor, D.; Weng, G.; Chao, H.; Rothberg, L.; Jedju, T. M.; Alfano, R. R.; Callender, R. H. *Proc. Natl. Acad. Sci. U.S.A.* **1991**, *88*, 9809.
(13) Peteanu, L. A.; Schoenlein, R. W.; Wang, Q.; Mathies, R. A.; Shank, C. V. *Proc. Natl. Acad. Sci. U.S.A.* **1993**, *90*, 11762.
(14) Schoenlein, R. W.; Peteanu, L. A.; Wang, Q.; Mathies, R. A.; Shank, C. V. *J. Phys. Chem.* **1993**, *97*, 12087.
(15) Kochendoerfer, G. G.; Mathies, R. A. *Isr. J. Chem.* **1995**, *35*, 211.
(16) Wang, Q.; Schoenlein, R. W.; Peteanu, L. A.; Mathies, R. A.; Shank, C. V. *Science* **1994,** *266*, 422.
(17) Heller, E. J.; Sundberg, R. L.; Tannor, D. *J. Phys. Chem.* **1982**, *86*, 1822.
(18) Elsaesser, T.; Kaiser, W. *Annu. Rev. Phys. Chem.* **1991**, *42*, 83. Doig, S. J.; Reid, P. J.; Mathies, R. A. *J. Phys. Chem.* **1991**, *95*, 6372.
(19) Palings, I.; Pardoen, J. A.; van den Berg, E.; Winkel, C.; Lugtenburg, J.; Mathies, R. A. *Biochemistry* **1987**, *26*, 2544.
(20) Applebury, M. L.; Zuckerman, D. M.; Lamola, A. A.; Jovin, T. M. *Biochemistry* **1974**, *13*, 3448.
(21) Oseroff, A. R.; Callender, R. H. *Biochemistry* **1974**, *13*, 4243.
(22) Mathies, R. A.; Oseroff, A. R.; Stryer, L. *Proc. Natl. Acad. Sci. U.S.A.* **1976**, *73*, 1.
(23) Champion, P. M.; Lange, R. *J. Chem. Phys*. **1980**, *73*, 5947.
(24) The 90° differential Raman cross sections are related to the absolute Raman cross section by $(8\pi/3)(1 + 2\rho)/(1 + \rho)$, where $\rho = 0.16$ is the depolarization ratio of the water bands at 3300 cm^{-1}.
(25) Strickler, S. J.; Berg, R. A. *J. Chem. Phys.* **1962**, *37*, 814.
(26) The following values were used for the absolute water Raman cross section for the bands at around 3300 cm^{-1} (in $Å^2$/molecule): 5.6×10^{-13} at 568.2 nm, 8.48×10^{-13} at 514.5 nm, and 13.2×10^{-13} at 472.7 nm.
(27) Guzzo, A. V.; Pool, G. L. *Science* **1968**, *159*, 312.
(28) Tallent, J. R.; Hyde, E. W.; Findsen, L. A.; Fox, G. C.; Birge, R. R. *J. Am. Chem. Soc.* **1992**, *114*, 1581.
(29) Shreve, A. P.; Trautman, J. K.; Owens, T. G. ; Albrecht, A. C. *Chem. Phys. Lett.* **1991**, *178*, 89.
(30) Kandori, H.; Sasabe, H.; Mimuro, M. *J. Am. Chem. Soc*. **1994**, *116*, 2671.
(31) Myers, A. B.; Harris, R. A.; Mathies, R. A. *J. Chem. Phys.* **1983**, *79*, 603.
(32) Lewis, A.; Spoonhower, J. P.; Perreault, G. J. *Nature (London)* **1976**, *260*, 675.
(33) Polland, H.-J.; Franz, M. A.; Zinth, W.; Kaiser, W.; Koelling, E.; Oesterhelt, D. *Biophys. J.* **1986**, *49*, 651.
(34) Du, M.; Fleming, G. R. *Biophys. Chem.* **1993**, *48*, 101.
(35) Lin, Steven W. T. Ph.D. Thesis, University of California at Berkeley, CA, 1994. Manuscript in preparation.
(36) Hudson, B. S.; Kohler, B. E.; Schulten, K. In *Excited States*; Lim, E. C., Ed.; Academic Press: New York, 1982; p 1.
(37) Birge, R. R. *Biochim. Biophys. Acta* **1990**, *1016*, 293.
(38) Eyring, G.; Curry, B.; Broek, A.; Lugtenburg, J.; Mathies, R. A. *Biochemistry* **1982**, *21*, 384.
(39) Wang, Q.; Kochendoerfer, G. G.; Schoenlein, R. W.; Verdegem, P. J. E.; Lugtenburg, J.; Mathies, R. A.; Shank, C. V. *J. Phys. Chem.*, submitted, and our unpublished results.
(40) Shreve, A. P.; Mathies, R. A. *J. Phys. Chem.* **1995**, *99*, 7285.
(41) Landau, L. D. *Phys. Z. Sowjetunion* **1932**, *2*, 46.
(42) Zener, C. *Proc. R. Soc. London, Ser. A* **1932**, *137*, 696.

JP960509+